Preprints of the 21st IFAC World Congress (Virtual)
Berlin, Germany, July 12-17, 2020

Model Predictive Control of Half-Car Active Suspension Systems Using Particle Swarm Optimisation

Jimoh.O, Pedro * **Sakhile.M.S, Nhlapo** **
Lindokuhle.J, Mpanza ***

* *School of Mechanical, Industrial and Aeronautical Engineering,University of the Witwatersrand, 1 Jan Smuts Avenue, Private Bag 03, Johannesburg WITS 2050, South Africa (e-mail 1: Jimoh.Pedro@wits.ac.za, e-mail 2: Jimoh.Olarewaju.Pedro@gmail.com).*
** *(e-mail: shakesnhlapo@gmail.com)*
*** *(e-mail: ljmpanza@gmail.com)*

Abstract: This paper presents the design of a particle swarm-optimised model predictive controller (MPC) for a half-car nonlinear electrohydraulic suspension system as it traverses a deterministic road disturbance. The particle swarm optimisation (PSO) algorithm uses an objective function which is based on conflicting active vehicle suspension system (AVSS) design specifications such as: ride comfort, road holding, road handling, suspension travel and power consumption. An inner-loop PID-based force feedback control is incorporated in the design to ensure good force tracking. The half-car model is composed of nonlinear suspensions and actuator dynamics. Simulation results demonstrate the superior performance of the proposed control scheme over the passive vehicle suspension system (PVSS) and the non-optimised MPC in rejecting the deterministic road disturbance.

Keywords: Particle Swarm Optimisation, Model Predictive Control, Active Vehicle Suspension System, Electrohydraulic Actuator Dynamics, Cascaded Control

1 Introduction

The requirement to simultaneously increase road holding and ride comfort is a problem which constantly troubles the designers of passive vehicle suspension system (PVSS) as these two goals are at odds with one another. It is therefore customary of the PVSS designer to make an optimal trade-off between road holding and ride comfort (Thaller et al., (2016); Sharp and Crolla (1987)).

AVSS has been successfully utilised in the partial decoupling of road holding and ride comfort so that they may both be simultaneously improved. However, tuning the controller gains still remains an issue, the controller tuning complexity increases with the amount of adjusted parameters/gains, number of controllers used and sophistication of the controllers utilised (Bemporad et al., (2010)).

Proportional, Integral and Derivative (PID) control has been used in AVSS with success. It is possible to tune the PID controller by intuition when the plant model is linear, but for nonlinear systems a great deal of intuitive reasoning, experience and rigorous fine-tuning is required in order to achieve satisfactory results (Dangor et al., (2014)). PID control is the most prevalent controller and tuning methods such as Ziegler-Nichols and Cohen-Coon may be used to aid in the selection of gains (Dahunsi and Pedro (2015); Noris (2006)).

For nonlinear systems, using Ziegler-Nichols and Cohen-Coon methods only serves to give a reasonable initial approximation of the gains; it is then required of the control engineer to refine the gains. Heuristic optimisation principles such as controlled random search (CRS), genetic algorithm (GA), differential evolution (DE), pattern search (PS) and PSO have been used to refine PID-controller gains for AVSS purposes (Dangor et al., (2014); Ou and Lin (2006)).

Model predictive control (MPC) is a powerful control method which combines optimisation with preview capabilities, it can also enforce plant input and output constraints (Bemporad et al., (2010)). MPC was traditionally used in the chemical process industry because the slow system dynamics allowed online optimisation to be completed before the next time step (Garriga and Soroush (2010)). Modern computers have more processing power and it is now possible to use MPC for system with fast varying dynamics, such as AVSS (Rathai et al., (2018); Gohrle et al., (2012)).

MPC is therefore an attractive and feasible controller for AVSS purposes, however it has not enjoyed widespread usage in this field (Nguyen et al., (2016)). This can be partially attributed to the difficulty involved in attaining an accurate linear system model, which the MPC uses for forecasting purposes, and the complexity associated with tuning the MPC parameters.

The model predictive controller found in Matlab Simulink has 7 key parameters that can be varied to tune the MPC (MathWorks (2019)). More often than not, only the sample time, prediction horizon and control horizon are varied when tuning the controller. Meaning that the full potential of the MPC is not exploited. Manually tuning such a high number of parameters accurately is a tedious task and the likelihood of obtaining the best parameters for the system is reduced.

This paper presents the tuning of MPC and PID parameters using particle swarm optimisation (PSO) algorithm to control nonlinear suspension system with actuator dynamics in order to simultaneously improve ride comfort and road holding. The paper is organized as follows: the system model is presented in Section 2. Section 3 introduces controller implementation which also includes performance specifications and implementation of the PSO algorithm. Section 4 presents simulation results with discussion and the paper is concluded in Section 5.

2 System Overview and Modelling

Figure 1 depicts the half-car schematic used in this paper. The front and rear springs and dampers are fitted between the half-car sprung mass and unsprung masses respectively.

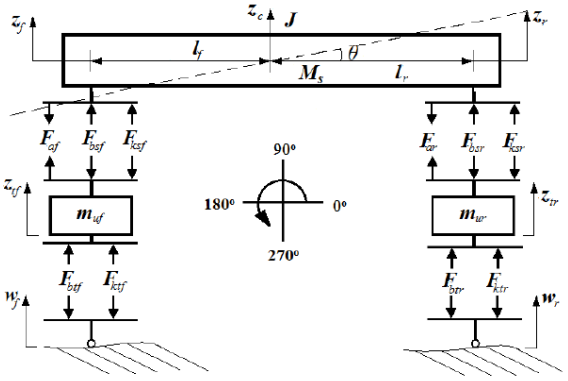

Fig. 1: Half-car schematic

The front and rear sprung mass displacements are given respectively as (Ekoru and Pedro (2013)):

$$z_f = z_c - l_f \sin\theta; \quad z_r = z_c + l_r \sin\theta, \tag{1}$$

where z_c and θ are the vertical and angular displacements of the sprung mass, l_f and l_r are the distances measured from the centre of gravity up to the chassis front and rear respectively. The front and rear velocities of the chassis are given respectively as:

$$\dot{z}_f = \dot{z}_c - l_f\dot{\theta}\cos\theta; \quad \dot{z}_r = \dot{z}_c + l_r\dot{\theta}\cos\theta, \tag{2}$$

where $\dot{z}_c$ and $\dot{\theta}$ are the vertical and angular velocities of the sprung mass. The front and rear suspension stiffness forces are represented by F_{ksf} and F_{ksr} which are described respectively as:

$$\begin{aligned} F_{ksf} &= k_f^l(z_{tf} - z_f) + k_f^{nl}(z_{tf} - z_f)^3, \\ F_{ksr} &= k_r^l(z_{tr} - z_r) + k_r^{nl}(z_{tr} - z_r)^3, \end{aligned} \tag{3}$$

where k_f^l and k_r^l are the linear spring stiffnesses, k_f^{nl} and k_r^{nl} are the nonlinear spring stiffnesses and $(z_{tf} - z_f)$ and $(z_{tr} - z_r)$ are the suspension travel for the front and rear respectively. The front and rear damping forces, F_{bsf} and F_{bsr} are given respectively as:

$$\begin{aligned} F_{bsf} =& b_f^l(\dot{z}_{tf} - \dot{z}_f) - b_f^{sym}|\dot{z}_{tf} - \dot{z}_f| + \\ & b_f^{nl}sgn(\dot{z}_{tf} - \dot{z}_f)\sqrt{|\dot{z}_{tf} - \dot{z}_f|}; \\ F_{bsr} =& b_r^l(\dot{z}_{tr} - \dot{z}_r) - b_r^{sym}|\dot{z}_{tr} - \dot{z}_r| + \\ & b_r^{nl}sgn(\dot{z}_{tr} - \dot{z}_r)\sqrt{|\dot{z}_{tr} - \dot{z}_r|}, \end{aligned} \tag{4}$$

where b_f^l and b_r^l are the linear damping, b_f^{sym} and b_r^{sym} are the asymmetric damping, b_f^{nl} and b_r^{nl} are the nonlinear damping and $(\dot{z}_{tf} - \dot{z}_f)$ and $(\dot{z}_{tr} - \dot{z}_r)$ are the suspension velocity for the front and rear respectively.

The tyre forces due to stiffness, F_{ktf} and F_{ktr}, are given respectively as:

$$F_{ktf} = k_{tf}(z_{tf} - w_f); \quad F_{ktr} = k_{tr}(z_{tr} - w_r), \tag{5}$$

where k_{tf} and k_{tr} are the tyre stiffness, w_f and w_r are the road profile and $(z_{tf} - w_f)$ and $(z_{tr} - w_r)$ are the tyre deflections for the front and rear respectively. The tyre damping forces F_{btf} and F_{btr} are respectively given as:

$$F_{btf} = b_{tf}(\dot{z}_{tf} - \dot{w}_f); \quad F_{btr} = b_{tr}(\dot{z}_{tr} - \dot{w}_r), \tag{6}$$

where b_{tf} and b_{tr} are the tyre damping constants, $\dot{w}_f$ and $\dot{w}_r$ are the road profile time derivatives and $(\dot{z}_{tf} - \dot{w}_f)$ and $(\dot{z}_{tr} - \dot{w}_r)$ are tyre deflection time derivatives for the front and rear respectively. The electrohydraulic actuator governing equations are given as:

$$\dot{x}_{vi} = \frac{1}{\tau}(-x_{vi} + K_i \cdot u_i), \tag{7}$$

where x_{vi} is the spool-valve displacement, τ is the servo time constant, $\dot{x}_{vi}$ is the spool-valve velocity, K_i is the servo gain factor and u_i is the input voltage from a controller, the subscript i will be replaced by f for front and r for rear respectively. The pressure time derivative is represented by $\dot{P}_{li}$ and is given as:

$$\dot{P}_{li} = \gamma Q_i - \beta P_{li} + \alpha A_{hyd}(\dot{z}_{ti} - \dot{z}_i), \tag{8}$$

where $\alpha = \frac{4\beta_e}{V_t}$, $\beta = C_{tp}\frac{4\beta_e}{V_t}$ and $\gamma = C_{dis}\cdot\Omega\cdot\sqrt{\frac{1}{\rho}}\frac{4\beta_e}{V_t}$ where C_{dis} is the discharge coefficient, Ω is the spool-valve area gradient, ρ is the hydraulic fluid density, β_e is the bulk modulus, V_t is the actuator total volume, C_{tp} is the leakage coefficient, P_{li} is the pressure applied on the piston face and A_{hyd} is the piston area. The flowrate is given as:

$$Q_i = x_{vi} \cdot sgn[P_s - sgn(x_{vi})P_{li}]\sqrt{|P_s - sgn(x_{vi})P_{li}|} \tag{9}$$

where P_s is the supply pressure. The respective actuator force is then given as:

$$F_{ai} = A_{hyd} \cdot P_{li}. \tag{10}$$

The front and rear active vehicle suspension system forces are given respectively as:

$$f_{sf} = F_{ksf} + F_{bsf} - F_{af}; \quad f_{sr} = F_{ksr} + F_{bsr} - F_{ar}, \tag{11}$$

where F_{af} and F_{ar} are the front and rear actuator forces respectively. The tyre forces for the front and rear are summed up and expressed as:

$$f_{tf} = F_{ktf} + F_{btf}; \quad f_{tr} = F_{ktr} + F_{btr}, \tag{12}$$

where f_{tf} and f_{tr} are the front and rear tyre forces respectively. Equations (13) - (16) are the acceleration terms of the four half-car degrees-of-freedom:

$$\ddot{z}_c = \frac{1}{M_s}(f_{sf} + f_{sr}), \tag{13}$$

$$\ddot{\theta} = \frac{1}{I_\theta}(-l_f \cdot f_{sf} \cdot \cos\theta + l_r \cdot f_{sr} \cdot \cos\theta), \tag{14}$$

$$\ddot{z}_{ft} = \frac{1}{M_{ft}}(-f_{sf} - f_{tf}) \text{ and} \tag{15}$$

$$\ddot{z}_{rt} = \frac{1}{M_{rt}}(-f_{sr} - f_{tr}), \tag{16}$$

where $\ddot{z}_c$ and $\ddot{\theta}$ are the heave and pitching accelerations of the sprung mass and M_s is the sprung mass. $\ddot{z}_{ft}$ and $\ddot{z}_{rt}$ are the front and rear unsprung mass heave accelerations, while M_{ft} and M_{rt} are the front and rear unsprung masses respectively.

The selected deterministic disturbance consists of a single sinusoidal half wave, the equations describing it are given as (Ekoru and Pedro (2013)):

$$w_f = \begin{cases} \frac{a}{2}\left(1 - \cos(\frac{2\pi V t}{\lambda})\right) & \text{if } 1 \le t \le (1 + \frac{\lambda}{V}), \\ 0 & \text{otherwise,} \end{cases} \tag{17}$$

$$w_r = \begin{cases} \frac{a}{2}\left(1 - \cos(\frac{2\pi V t}{\lambda})\right) & \text{if } (1 + t_d) \le t \le \\ & (1 + t_d + \frac{\lambda}{V}), \\ 0 & \text{otherwise,} \end{cases} \tag{18}$$

where w_f and w_r are the front and rear road displacements respectively, a is the hump amplitude, V is the velocity of the vehicle and remains constant through each simulation, t is the time and λ is the hump half-wavelength. Time delay is represented by t_d, it is the time by which the rear wheel lags the front wheel, it is expressed as:

$$t_d = \frac{l_f + l_r}{V} \tag{19}$$

the deterministic disturbance and AVSS half-car parameters are the same as described in (Ekoru and Pedro (2013)).

The AVSS governing equations can be expressed in state-space format as:

$$\dot{\mathbf{x}} = \mathbf{f(x)} + \mathbf{g(x)u} + \mathbf{p} \cdot \mathbf{w}, \tag{20}$$

where $\mathbf{(x)}$ is the state vector, $\mathbf{g(x)}$ is the control input matrix, $\mathbf{u}$ is the control input vector, $\mathbf{p}$ is the disturbance input matrix and $\mathbf{w}$ is the disturbance input vector. The state vector, $\mathbf{x}$, is given as:

$$\begin{aligned} \mathbf{x} &= [z_c, \theta, z_{tf}, z_{tr}, \dot{z}_c, \dot{\theta}, \dot{z}_{tf}, \dot{z}_{tr}, P_{lf}, P_{lr}, x_{vf}, x_{vr}]^T \\ &= [x_1, x_2, x_3, x_4, x_5, x_6, x_7, x_8, x_9, x_{10}, x_{11}, x_{12}]^T, \end{aligned} \tag{21}$$

the control input vector is given as:

$$\mathbf{u} = [V_{control_1}, V_{control_2}]^T = [u_1, u_2]^T, \tag{22}$$

the disturbance input vector is given as:

$$\mathbf{w} = [w_f, w_r, \dot{w}_f, \dot{w}_r]^T, \tag{23}$$

the output vector is given as:

$$\mathbf{y} = \mathbf{h(x)} = \begin{bmatrix} x_3 - x_1 + l_f \sin x_2 \\ x_4 - x_1 - l_r \sin x_2 \end{bmatrix}. \tag{24}$$

3 Controller Implementation

The objective function is specified in such a way that when it is minimised, the road holding and ride comfort are improved over the PVSS case, the specifications selected are based on the physical limits of the system (Dangor et al., (2014)). The performance index is given as:

$$\begin{aligned} J &= J_1 + J_2 + J_3 + J_4 + J_5 \\ &= \frac{1}{T}\int_0^T \left[\left(\frac{\ddot{z}_c}{\ddot{z}_{c_{max}}}\right)^2 + \left(\frac{\ddot{\theta}}{\ddot{\theta}_{max}}\right)^2\right] dt + \\ &\frac{1}{T}\int_0^T \left[\left(\frac{F_{tf}}{F_{tf_{max}}}\right)^2 + \left(\frac{F_{tr}}{F_{tr_{max}}}\right)^2\right] dt + \\ &\frac{1}{T}\int_0^T \left[\left(\frac{y_f}{y_{f_{max}}}\right)^2 + \left(\frac{y_r}{y_{r_{max}}}\right)^2\right] dt + \\ &\frac{1}{T}\int_0^T \left[\left(\frac{u_f}{u_{f_{max}}}\right)^2 + \left(\frac{u_r}{u_{r_{max}}}\right)^2\right] dt + \\ &\frac{1}{T}\int_0^T \left[\left(\frac{F_{af}}{F_{af_{max}}}\right)^2 + \left(\frac{F_{ar}}{F_{ar_{max}}}\right)^2\right] dt, \end{aligned} \tag{25}$$

where J_1 pertains to ride comfort and vehicle handling while $\ddot{z}_{c_{max}}$ and $\ddot{\theta}_{max}$ are the maximum permitted chassis heave and pitching accelerations respectively, J_2, J_3, J_4 and J_5 address dynamic tyre forces, suspension travel, controller voltage and actuator force respectively, the subscript max refers to the maximum allowable value of each respective entity.

3.1 Particle Swarm Optimization

PSO is a random search optimisation routine which searches a predetermined area of feasibility with the aim of minimising the performance index given by Equation (25). Each PSO particle individually explores the area of feasibility, with the expectation that as the number of iterations increases, all particles will migrate towards one point, which is the minimum of the performance index J (Mpanza and Pedro (2016)). The area of feasibility is defined through intuitive reasoning and experience gained through manual tuning (Pedro et al., (2018)), in this instance, it is specified by defining upper and lower limits for each gain/parameter. The PSO algorithm is as described in (Dangor et al., (2014)).

The optimisation is carried out offline by iteratively computing the position of each particle using:

$$\mathbf{x}(t+1) = \mathbf{x}(t) + \mathbf{V}(t+1) \tag{26}$$

where $\mathbf{x}$ is the position vector of each particle and $\mathbf{V}$ is the velocity vector, it randomly determines how far a particle moves during the particular iteration, $\mathbf{V}$ is defined as:

$$\begin{aligned} \mathbf{V}(t+1) =& w\mathbf{V}(t) + r_1 c_1(\mathbf{P}_{best} - \mathbf{x}(t)) + \\ & r_2 c_2(\mathbf{G}_{best} - \mathbf{x}(t)) \end{aligned} \tag{27}$$

where $\mathbf{G}_{best}$ is the set of problem variables that produced the best global results thus far, $\mathbf{P}_{best}$ is a matrix containing the individual best positions of each particle, $(\mathbf{P}_{best} - \mathbf{x}(t))$ is called the local search vector and $(\mathbf{G}_{best} - \mathbf{x}(t))$ is the global search vector, w is the inertia weight, c_1 and c_2 are the learning rates, r_1 and r_2 are uniformly distributed random numbers between 0 and 1.

The PSO algorithm can be carried out for a specified number of iterations or until certain stopping criterion, such as gain standard deviation, are reached (Pedro et al., (2018)). PSO was used separately for the inner and

outer loop, beginning with the inner loop, to determine the optimal gains. The number of iterations was specified as 150 and the PSO parameters used are: $w = 0.7$, $c_1 = 2$ and $c_2 = 3$ respectively.

3.2 PID Controller Design

The half-car AVSS consists of two control loops, an inner loop to control the actuator force and an outer loop to control suspension travel. The inner loop utilises parallel PID controllers, time domain representations and error signal are given respectively as:

$$F_{desired_i}(t) = \left(K_P + K_I \int dt + K_D \frac{d}{dt}\right) e(t), \quad (28)$$

$$e = R - (z_{ti} - z_i), \quad (29)$$

where K_P, K_I and K_D are the proportional, integral and derivative gains respectively, i denotes either front or rear, R is the reference suspension travel and $(z_{ti} - z_i)$ is the suspension travel at the front or rear. The PID gains were initially selected by manual tuning, thereafter they were refined using PSO to minimise the performance index J. Table 1 gives the values of the PID gains, ISO2631 − 1 comfort rating and performance index for the manually and PSO-tuned PIDs (Plewa et al., (2012)).

Table 1. PID inner-loop gains

Technique	Station	K_P	K_I	K_D	ISO2631 − 1	J
Manual	Front	0.01667	1	4×10^{-4}	0.2489	0.1206
	Rear	0.01667	1	4×10^{-4}		
PSO	Front	0.0045	1.3701	4×10^{-4}	0.2485	0.1202
	Rear	0.0044	1.1788	3×10^{-4}		

3.3 MPC Controller Design

The half-car outer control loop utilises two MPC controllers for maintaining the desired suspension travel; the required suspension travel is set to $0m$, therefore making this a regulation control problem. The MPC controller determines the relevant future manipulated variable by minimising the following performance index (Zhao and Zhu (2019)):

$$J_{MPC} = \sum_{i=1}^{p} Q_y(y(k+i) - w(k+i))^2 + \sum_{i=1}^{m} R_u \Delta u^2(k+j-1), \quad (30)$$

where $Q_y = diag(q_1\ q_2 \cdots\ q_p)$ and $R_u = diag(r_1\ r_2 \cdots\ r_m)$ respectively. The Q_y and R_u matrices are the weight matrices of the output and manipulated variables respectively.

The MPC approach is described as in (Zhao and Zhu (2019)):

$$\begin{aligned} x(k+1) &= Ax(k) + B_u u(k) + B_v v(k) + B_d k, \\ y_u(k) &= C_u x(k) + D_{uu} u(k) + D_{du} d(k), \\ y_m(k) &= C_m x(k) + D_{vm} v(k) + D_{dm}(k), \end{aligned} \quad (31)$$

where $y_u(k)$ is the unmeasured system output, $y_m(k)$ is the measured system output, u_k is the manipulated variable, v_k is the measured disturbance and $d(k)$ is the unmeasured disturbance.

Table 2 gives the MPC parameters, ISO2631 − 1 comfort rating and performance index for the manually and PSO-tuned MPCs,

Table 2. MPC outer-loop parameters

Technique	Manual		PSO	
Station	Front	Rear	Front	Rear
MV_s	10	10	33.102	32.510
OV_s	6.000×10^{-4}	6.000×10^{-4}	6.724×10^{-4}	6.930×10^{-4}
MV_{wr}	3.300×10^{-3}	3.300×10^{-3}	8.200×10^{-3}	2.570×10^{-2}
OV_w	1.205	1.205	4.409	3.629
ECR_w	1.205×10^5	1.205×10^5	1.730×10^6	5.439×10^6
P	100	100	115	83
N	10	10	24	12
ISO2631 − 1	0.2485		0.2022	
J	0.1202		0.0872	

where MV_s and MV_{wr} are the manipulated variable scale factor and weight rate respectively; OV_s and OV_w are the output variable scale factor and weight respectively; ECR_w is the equal concern for relaxation weight while P and N are the prediction and control horizons respectively, the MPC sampling time was constant at $0.001s$. Convergence of the performance index is shown in Figure 2.

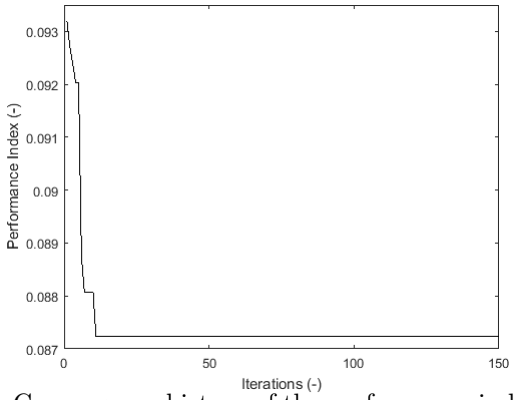

Fig. 2: Convergence history of the performance index with number of iterations

The performance index value evolved 7 times to converge to 0.0872 by the 11^{th} iteration, optimisation is carried out for each iteration. Figure 3 depicts the half-car control structure.

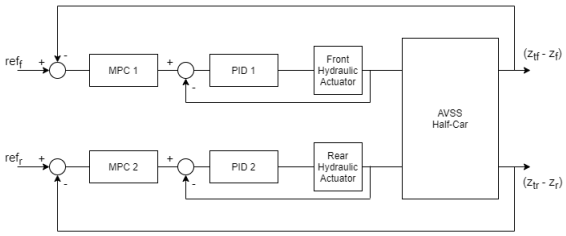

Fig. 3: Half-car control structure

The mean and standard deviation were determined for the convergence history of the MPC parameters, which are given in Table 3.

Table 3. Mean and Standard Deviation for MPC Paremeters

Station	Front		Rear	
Entity	Mean	SD	Mean	SD
MV_s	33.084	0.222	32.014	1.941
OV_s	6.760×10^{-4}	0.030×10^{-3}	6.970×10^{-4}	0.025×10^{-3}
MV_{wr}	8.200×10^{-3}	1.800×10^{-3}	2.580×10^{-2}	3.8000×10^{-3}
OV_w	4.371	0.368	3.622	0.425
ECR_w	1.732×10^6	0.182×10^6	5.256×10^6	0.738×10^6
P	115.033	1.529	85.960	11.255
N	23.800	1.217	12.027	0.229

4 Results and Discussion

Performance of the half-car AVSS was assessed as it traversed a deterministic road disturbance at a constant

velocity of $40km/h$, the simulations were carried out in Matlab/Simulink.

Figure 4 depicts the half-car suspension travel. Irrespective of the control technique, addition of AVSS has a significant impact on reducing suspension travel and lowering settling time. PSO-MPC outperformed MPC by a noticeable degree as far as suspension travel is concerned, resulting in smaller peak-to-peak values and a substantially shorter settling time.

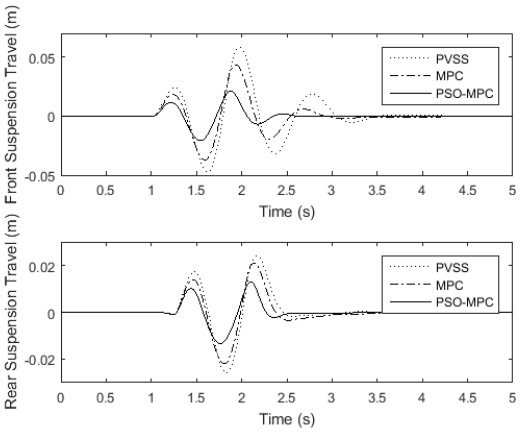

Fig. 4: Suspension travel response for PVSS, MPC, and PSO-MPC cases

Figure 5 depicts the half-car dynamic tyre force. Initially the front PSO-MPC produces peak values that are slightly larger than those of PVSS and MPC, midway through the front transient response MPC and PSO-MPC both perform noticeably better than PVSS, indicating improved road holding in the latter part of the transient response. Addition of AVSS to the rear caused deteriorated performance irrespective of the control type.

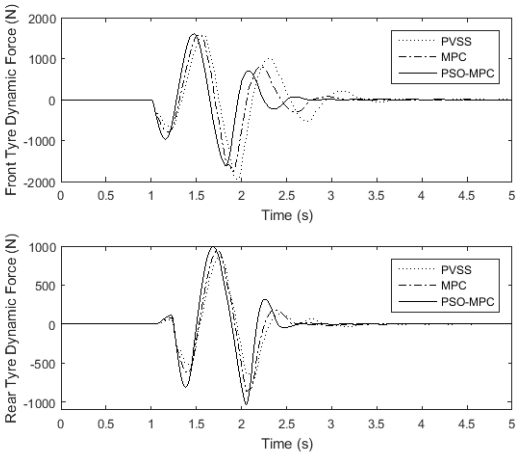

Fig. 5: Dynamic tyre force response for PVSS, MPC, and PSO-MPC cases

Figures 6 and 7 depict the half-car AVSS actuator force and controller voltage. In some instances, the front PSO-MPC produced peak forces which were almost twice as large as MPC and all rear PSO-MPC actuation forces were over twice as large as MPC. Settling time was improved by using PSO-MPC, it was reduced from $3.5s$ to $2.8s$ for the front and $3.4s$ to $2.6s$ for the rear respectively.

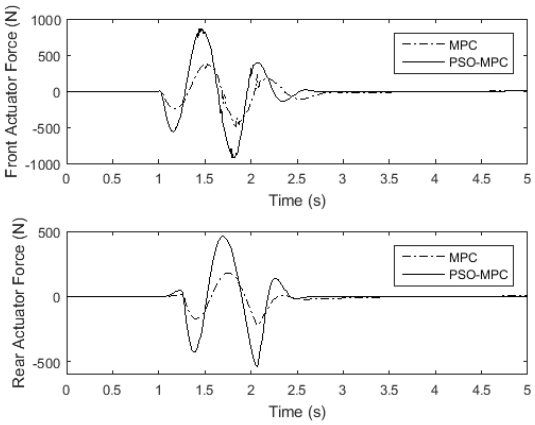

Fig. 6: Actuator force response for MPC and PSO-MPC cases

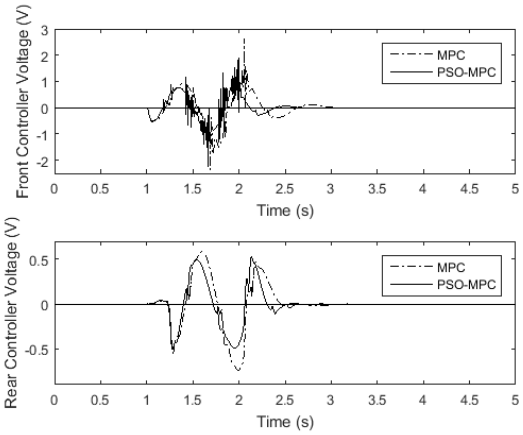

Fig. 7: Control input voltage response for MPC and PSO-MPC cases

The front actuator voltage for PSO-MPC contains a considerable amount of chattering and spiking, despite this, the actuator output force is substantially smoother and only displays very slight chattering at its two most extreme values. Smoothing out of the actuator voltage can be attributed to the low-pass filter which forms part of the actuator dynamics; it removes effects of high-frequency changes in actuator input voltage.

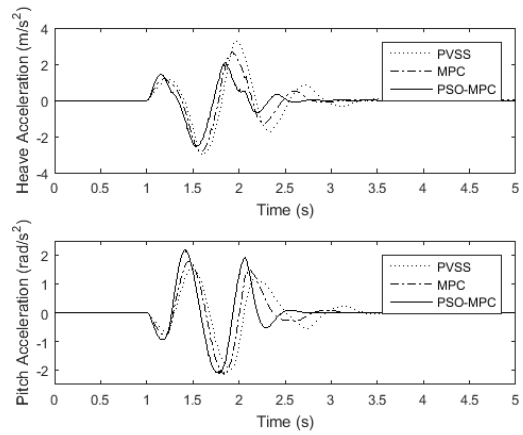

Fig. 8: Sprung mass heave and pitch accelerations response for PVSS, MPC and PSO-MPC cases

Figure 8 depicts the sprung mass heave and pitch accelerations respectively. The initial peak heave acceleration value is highest for PSO-MPC but thereafter PSO-MPC manages to reduce peak heave acceleration values considerably, outperforming both MPC and PVSS. PSO-MPC also produced the smallest settling time for both sprung mass heave and pitch accelerations respectively. Use of AVSS resulted in increased peak pitch acceleration forces, which resulted in deteriorated road handling abilities. Table 4 gives the ISO2631 − 1 weighted RMS values of the half car.

Table 4. ISO2631 − 1 weighted RMS results

Technique	Weighted RMS	ISO2631 − 1 designation	Difference Δ
PVSS	0.290	Not Uncomfortable	–
MPC	0.249	Not Uncomfortable	+14.14%
PSO-MPC	0.202	Not Uncomfortable	+30.34%

The weighting factor which was utilised is 0.4, it corresponds to measurements taken at the passengers' feet as the half-car modelled in this paper does not have seats. All three of the simulations resulted in low enough weighted RMS heave acceleration values that they rank in the ISO2631 − 1 highest level for comfort, which is *not uncomfortable*. Despite ranking in the highest level of comfort, the use of AVSS was able to further increase comfort levels by +14.14% and +30.34% for MPC and PSO-MPC respectively when compared to PVSS.

5 Conclusions

The main outcomes of this paper are as follows:

- Use of PSO-MPC resulted in the performance index J being minimised and also improvements in ISO2631 − 1 comfort levels.
- A decoupling of ride comfort and road holding was observed at the front, both were simultaneously increased.
- Future work should include a performance index which is defined individually for the front and rear suspension.
- Future work should also include the use of multiobjective particle swarm optimisation algorithm to select the MPC parameters.

6 References

Bemporad, A., Morari, M. and Ricker, N.L., 2010. Model Predictive Control Toolbox Users Guide. The mathworks.

Dahunsi, O.A. and Pedro, J.O., 2015. PID Reference Tracking Control for Nonlinear Active Vehicle Suspension System. In International Conference on Industrial Application Engineering (pp. 132-139).

Dangor, M., Dahunsi, O.A., Pedro, J.O. and Ali, M.M., 2014. Evolutionary algorithm-based PID controller tuning for nonlinear quarter-car electrohydraulic vehicle suspensions. Nonlinear dynamics, 78(4), pp.2795-2810.

Ekoru, J.E. and Pedro, J.O., 2013. Proportional-integral-derivative control of nonlinear half-car electro-hydraulic suspension systems. Journal of Zhejiang University SCIENCE A, 14(6), pp.401-416.

Garriga, J.L. and Soroush, M., 2010. Model predictive control tuning methods: A review. Industrial Engineering Chemistry Research, 49(8), pp.3505-3515.

Gohrle, C., Wagner, A., Schindler, A. and Sawodny, O., 2012, June. Active suspension controller using MPC based on a full-car model with preview information. In 2012 American Control Conference (ACC) (pp. 497-502). IEEE.

MathWorks. 2019. mpc. [ONLINE] Available at: https://www.mathworks.com/help/mpc/ref/mpc.html. [Accessed 16 October 2019].

Mpanza, L.J. and Pedro, J.O., 2016, October. Sliding mode control parameter tuning using ant colony optimization for a 2-DOF hydraulic servo system. In 2016 IEEE International Conference on Automatic Control and Intelligent Systems (I2CACIS) (pp. 242-247). IEEE.

Nguyen, M.Q., Canale, M., Sename, O. and Dugard, L., 2016, December. A Model Predictive Control approach for semi-active suspension control problem of a full car. In 2016 IEEE 55th Conference on Decision and Control (CDC) (pp. 721-726). IEEE.

Noris, M.F., 2006. Comparison between Ziegler− Nichols and Cohen−Coon Method for Controller Tunings. Faculty of Chemical Natural Resources Engineering, University College of Engineering Technology Malaysia, MS Thesis.

Ou, C. and Lin, W., 2006, June. Comparison between PSO and GA for parameters optimization of PID controller. In 2006 International conference on mechatronics and automation (pp. 2471-2475). IEEE.

Pedro, J.O., Dangor, M., Dahunsi, O.A. and Ali, M.M., 2018. Dynamic neural network-based feedback linearization control of full-car suspensions using PSO. Applied Soft Computing, 70(1), pp.723-736.

Plewa, K.M., Eger, T.R., Oliver, M.L. and Dickey, J.P., 2012. Comparison between ISO 26311 Comfort Prediction Equations and Self-Reported Comfort Values during Occupational Exposure to Whole-Body Vehicular Vibration. Journal of Low Frequency Noise, Vibration and Active Control, 31(1), pp.43-53.

Rathai, K.M.M., Alamir, M., Sename, O. and Tang, R., 2018. A parameterized NMPC scheme for embedded control of semi-active suspension system. IFAC-PapersOnLine, 51(20), pp.301-306.

Sharp, R.S. and Crolla, D.A., 1987. Road vehicle suspension system design-a review. Vehicle system dynamics, 16(3), pp.167-192.

Thaller, S., Reiterer, F., Schmied, R., Waschl, H., Kokal, H. and del Re, L., 2016. Fast determination of vehicle suspension parameters via continuous time system identification. IFAC-PapersOnLine, 49(11), pp.448-453.

Zhao, Q. and Zhu, B., 2019. Multi-objective optimization of active suspension predictive control based on improved PSO algorithm. Journal of Vibroengineering, 21(5), pp.1388-1404.